

Nanoscale

Accepted Manuscript



This is an *Accepted Manuscript*, which has been through the Royal Society of Chemistry peer review process and has been accepted for publication.

Accepted Manuscripts are published online shortly after acceptance, before technical editing, formatting and proof reading. Using this free service, authors can make their results available to the community, in citable form, before we publish the edited article. We will replace this *Accepted Manuscript* with the edited and formatted *Advance Article* as soon as it is available.

You can find more information about *Accepted Manuscripts* in the [Information for Authors](#).

Please note that technical editing may introduce minor changes to the text and/or graphics, which may alter content. The journal's standard [Terms & Conditions](#) and the [Ethical guidelines](#) still apply. In no event shall the Royal Society of Chemistry be held responsible for any errors or omissions in this *Accepted Manuscript* or any consequences arising from the use of any information it contains.

ARTICLE

Colloidal synthesis and optical properties of type-II CdSe-CdTe and inverted CdTe-CdSe core-wings heteronanoplatelets†

Cite this: DOI: 10.1039/x0xx00000x

Received 00th January 2012,
Accepted 00th January 2012

DOI: 10.1039/x0xx00000x

www.rsc.org/A. V. Antanovich,^a A. V. Prudnikau,^a D. Melnikau,^b Y. P. Rakovich,^{b,c}
A. Chuvilin,^{c,d} U. Woggon,^e A. W. Achtstein^e and M. V. Artemyev^{a*}

We develop the colloidal synthesis and investigate the structural and electronic properties of CdSe-CdTe and inverted CdTe-CdSe heteronanoplatelets and experimentally demonstrate that the overgrowth of cadmium selenide or cadmium telluride core nanoplatelets with counterpart chalcogenide wings leads to type-II heteronanoplatelets with emission energies defined by the bandgaps of the CdSe and CdTe platelets and the characteristic band offsets. The observed conduction and valence band offsets of 0.36 eV and 0.56 eV are in line with theoretical predictions. The presented type-II heteronanoplatelets exhibit efficient spatially indirect radiative exciton recombination with a quantum yield as high as 23%. While the exciton lifetime is strongly prolonged in the investigated type-II 2D systems with respect to 2D type-I systems, the occurring 2D Giant Oscillator Strength (GOST) effect still leads to a fast and efficient exciton recombination. This makes type-II heteronanoplatelets interesting candidates for low threshold lasing applications and photovoltaics.

Introduction

Semiconductor nanocrystals (NCs) in the strong confinement regime possess a variety of unique optical and electronic properties, which can be modified through altering size, shape and surface composition of NCs.^{1,2} In addition to that, the properties of NCs can also be varied through the preparation of various heteronanocrystals (HNCs). Depending on the relative position of the conduction (CB) and valence (VB) bands of the adjoining materials, the created heterojunctions can be divided into type-I and type-II ones when the bands of one NC are positioned within the energy gap of the other (type-I) or are staggered (type-II) with respect to the bandgap of the other.¹ HNCs prepared through colloidal synthesis usually have a core-shell architecture.³ Generally in the case of type-I HNCs a semiconductor core is covered with wider bandgap shell in order to protect the core from the interaction with the environment and provide a passivation of dangling bonds on the surface. This leads to simultaneous confinement of the electron and hole in the core resulting in an increased overlap of the carrier wavefunctions. Moreover, such structures are characterized by higher radiative recombination probabilities and stability against photodegradation, and thus increased PL quantum yields.⁴⁻⁶ Such HNCs are widely implemented as materials for light-emitting devices⁷ and bioimaging⁸ applications.

In the case of type-II heteronanostructures one of the charge carriers is confined in the core while another resides in the shell, since the lowest energy states for electron and hole are positioned in different parts of heterostructure.⁹ This spatial separation leads to reduced overlap of electron and hole wavefunctions and increased exciton state lifetime.¹⁰ The radiative recombination of the electron and hole occurs due to a spatially indirect transition which is red shifted with respect to both semiconductor band gaps. Such NCs exhibit optical properties different from those for type-I materials such as suppressed blinking and Auger recombination^{11,12} and increased multiexciton generation rates.¹³ This, in turn, allows lowering lasing thresholds,¹⁴ improving photovoltaic devices performance^{10,15} and utilization of these heterostructures in photocatalytic¹⁶ and biomedical applications.¹⁷ Generally, photovoltaic and photocatalytic applications require directional charge separation which could not be realized in the case of core-shell QDs. Therefore type-II HNCs with heterojunctions in 1D (quantum rods) or 0D (quantum dots) NCs like CdSe-CdTe nanorods and nanowires,¹⁸⁻²¹ CdSe-CdTe nanobarbells^{22,23} CdSe-CdTe tetrapods^{24,25} gained considerable attention. Semiconductor heteronanostructures were extensively studied in the case of epitaxially grown quantum wells and superlattices.²⁶ In contrast to various epitaxial growth procedures colloidal synthesis has become cheaper and more versatile method of heteronanostructures preparation, that, in

turn, allows the preparation of HNCs with complex composition and shape, such as heteronanorods, nanobarbells, tetrapods and multibranch architectures²⁷ and significantly increases their processability.

At the same time semiconductor NCs with 1D quantum confinement (quantum nanoplatelets, NPLs) composed of cadmium chalcogenides are currently being extensively studied^{28–32} and expected to be promising materials for the preparation of semiconductor HNCs with efficient charge separation. Such NPLs exhibit electronic and optical properties that differ from those for QDs, such as much narrower absorption and PL bands (FWHM < 10 nm), a giant oscillator strength, lower thresholds for amplified spontaneous emission and higher optical gain saturation.^{33–35}

However, the synthesis of heteronanostructures based on such nanoplatelets is limited to the preparation of CdSe-CdS or CdSe-CdZnS nanoparticles.^{36–38} Recently, we have shown that overgrowth of CdSe NPLs with CdS in the presence of acetate species results in the formation of NPLs with a “core-wings” architecture.³⁸ It was shown, that the thickness of CdS wings was the same (when expressed in monolayers) as the core thickness, what implies the epitaxial growth of the wings on the edges of the CdSe core. Both core-shell and core-wings CdSe-CdS heterostructured NPLs were shown to outperform bare CdSe NPLs as lasing and optical gain media and exhibit much superior properties as compared to semiconductor NPs of other dimensionalities.^{35,39,40} In this paper we further extend our approach reported earlier³⁸ on the preparation of type-II CdSe-CdTe core-wings heteronanoplatelets. During the submission of this manuscript we became aware of related works reporting of the realization of straight type-II CdSe-CdTe heteronanoplatelets obtained by different protocols.^{41–43} In these papers the authors demonstrate that the general approach for epitaxial overgrowth of flat CdSe core with CdTe wings results in characteristic type II optical transitions. Here, we demonstrate that not only straight CdSe-CdTe, but also inverted type II CdTe-CdSe core-wings system can be successfully obtained by the same method. We compare the optical properties of straight CdSe-CdTe and inverted CdTe-CdSe hetero-NPLs of the same thickness and show that both structures are complimentary to each other.

Experimental Section

Materials

Cadmium oxide, zinc acetate dihydrate, cadmium acetate dihydrate, n-trioctylphosphine, selenium and tellurium powder, myristic acid, oleic acid, octadecene-1 were purchased from Sigma-Aldrich and used as received.

Characterization techniques

Room temperature optical absorption spectra were recorded using HR-2000+ spectrometer (Ocean Optics) equipped with Ocean Optics DH-2000 white light source. Photoluminescence (PL) and photoluminescence excitation (PLE) measurements

were conducted with Jobin-Yvon Fluoromax-2 spectrofluorimeter. PL decay times were measured with PicoQuant Microtime200 fluorescence lifetime imaging confocal microscopy system. PL excitation was provided by picosecond laser pulses using PicoQuant LDH405 laser diode head controlled by Sepia II driver.

HRTEM imaging as well as EDX mapping was performed on Titan 60-300 (FEI, Netherlands) electron microscope equipped with xFEG emitter, monochromator, EDAX RTEM detector and imaging Cs corrector. The microscope was operated at 60kV in STEM mode for mapping and TEM mode for HR imaging. To provide sufficient EDX signal the gun lens was focused to provide approximately 0.5 nA beam current at nominal spotsize. The diameter of the spot at these conditions was about 2 nm. The 64x89 pixels spectrum image was acquired with a pitch of 1.9 nm and a dwell time of 0.3 s. Elemental maps and spectra were extracted later from thus acquired data cube.

Quantitative EDX analysis from the bulk powders was conducted using scanning electron microscope LEO-1420, equipped with an energy dispersive X-ray detector. Room temperature X-ray diffraction analysis of powdered samples of CdSe and CdSe-CdTe was carried out with Empyrean Series 2 diffractometer (Cu K_{α1} line). In order to remove any synthesis-related contaminants, prior to EDX and XRD studies NPLs were precipitated from chloroform solution by the addition of excess methanol, isolated by centrifugation and redispersed again in chloroform. This cycle was repeated several times and then NPLs were treated with tetrahydrofuran to remove the excess of ligands from the NPLs surface.

Synthetic procedures

Preparation of CdSe core nanoplatelets. CdSe NPLs with thicknesses of 5 monolayers were synthesized by modified procedures reported previously.^{34,44} Briefly, 35 mg of cadmium oxide, 165 mg of myristic acid and 15 ml of octadecene-1 were introduced in a three-necked flask and heated until cadmium oxide completely dissolved. After that the reaction flask cooled to the room temperature and 10 mg of selenium powder was added to the as-formed cadmium myristate solution. Then reaction flask was degassed, purged with argon and set to heat to 240 °C. At 193 °C 55 mg of zinc acetate dihydrate in powder was swiftly added into the reaction mixture. When the temperature reached 240 °C reaction flask was heated for 3 minutes. After this time heating mantle was removed and at 180 °C 1 ml of oleic acid was added to the reaction mixture. When reaction mixture cooled down to 80 °C CdSe core NPLs were precipitated out with isopropanol, isolated by centrifugation at 3000 rpm and redispersed in octadecene.

Preparation of CdSe-CdTe heteronanoplatelets. Freshly prepared purified CdSe NPLs, 113 mg (0.5 mmol) of cadmium acetate and 10 ml of ODE were mixed in a three-necked flask, degassed for 30 minutes at room temperature. After that the reaction flask was purged with argon and heated to 200 °C. At this temperature 0.5 ml of the mixture of Cd- and Te-precursor solutions was dropwise added into the CdSe core nanoplatelets

solution. Dropwise addition of precursors allows avoiding heterogeneous nucleation and promotes CdTe epitaxial deposition at the NPLs edges in the form of wings.

Cadmium precursor was prepared by heating 39 mg (0.3 mmol) of CdO and 255 μ l (0.8 mmol) of oleic acid in 3 ml ODE in argon. Tellurium precursor was prepared by dissolving 0.2 mmol of Te in the mixture of 2 ml ODE and 0.2 ml (0.4 mmol) TOP in argon. Prior to use the precursors were cooled to room temperature, mixed and transferred into a syringe under argon.

Preparation of CdSe 4ML core nanoplatelets. 4 ML thick CdSe NPLs were prepared according to the previously reported protocol.⁴⁴ A three-necked flask was charged with 92 mg of cadmium acetate, 8 mg Se powder, 32 μ l of oleic acid and 12 ml of octadecene-1. Then the flask was degassed for 15 minutes, purged with argon, heated to 180 °C and kept at this temperature for 15 minutes. After that the NPLs were isolated and purified in a similar fashion as the 5 ML thick CdSe NPLs.

Preparation of CdTe 4ML core nanoplatelets. CdTe NPLs with the thickness of 4 ML were prepared by a modified protocol reported before.³¹ Briefly, 0,3 mmol of cadmium acetate dihydrate, 0,45 mmol of oleic acid and 10 ml of ODE were introduced into three-necked flask and degassed at 90 °C for 30 minutes. After that flask was purged with argon and heated to 210 °C. At this point 200 μ l of 0.1 M TOP-Te solution in octadecene were swiftly injected and reaction mixture was heated for another 15 minutes to increase the reaction yield.

Preparation of CdSe(core)-CdTe(wings) NPLs and “inverted” CdTe(core)-CdSe(wings) nanoplatelets. CdTe “wings” deposition on the 4ML CdSe NPLs was performed by following the same protocol as one presented for 5ML thick CdSe NPLs. CdTe NPLs were laterally overgrown with CdSe “wings” following the similar procedure except that a suspension of elemental selenium in ODE was used as Se-source.

Results and Discussion

Absorption, PL, PLE

Fig. 1 shows optical absorption, PL and PLE spectra of 5 ML thick CdSe core NPLs before (a) and after (b) the lateral overgrowth with CdTe. One can see that after the overgrowth process absorption the features of the CdSe NPLs are retained and a new narrow excitonic band peaking at $\lambda = 556$ nm appears. This new transition is assigned to 5 ML (2.2 nm) thick CdTe NPLs.³¹ During the CdTe lateral overgrowth we did not observe any broadening of the peaks or considerable spectral shifts of the CdSe core absorption (it should be noted that the band centered at 510 nm for the CdSe-CdTe heteronanoparticles appears broader because of its overlap with the second excitonic band of CdTe). This allows assuming that the CdTe growth occurs at the edges of CdSe NPLs while their upper and lower planes remain unaffected because a lateral overgrowth of CdSe platelets with approx. 30 nm length does not result in a change of the lateral CdSe exciton confinement,³⁸ since the 2D exciton Bohr radius is only approx. 3 nm.³⁴ An

overgrowth of the CdSe basal planes would in contrast result in a strong shift of the exciton energy due to the weaker overall transversal confinement.

In the PL spectrum of the CdSe-CdTe hetero-NPLs we observe the vanishing of the CdSe PL band at $\lambda = 510$ nm and the appearance of new band at about $\lambda = 662$ nm. This considerably red-shifted band cannot be assigned either to CdSe, or to CdTe NPLs. Such a large red shift between the PL and absorption peaks of the CdSe and CdTe phases is a distinctive feature of type-II heterostructures. The formation of a type-II heterojunction is also supported by the fact that PLE spectrum of CdSe-CdTe NPLs registered at $\lambda_{\text{detect}} = 662$ nm (blue curve in Fig. 1b) follows well the absorption spectrum (black curve in Fig. 1b) thus indicating that PL emission originates from both the CdSe and CdTe phases. Similar behaviour was observed earlier for 4 and 5 ML CdSe-CdTe hetero NPLs prepared by different protocols.⁴¹⁻⁴³ The PL quantum yield of our 5 ML CdSe-CdTe HNPLs, measured at room temperature in chloroform relatively to Rhodamine 6G in ethanol, was 23%. That is a rather high value for the HNCs with an indirect optical transition schematically shown in Fig. 1c by a red arrow.

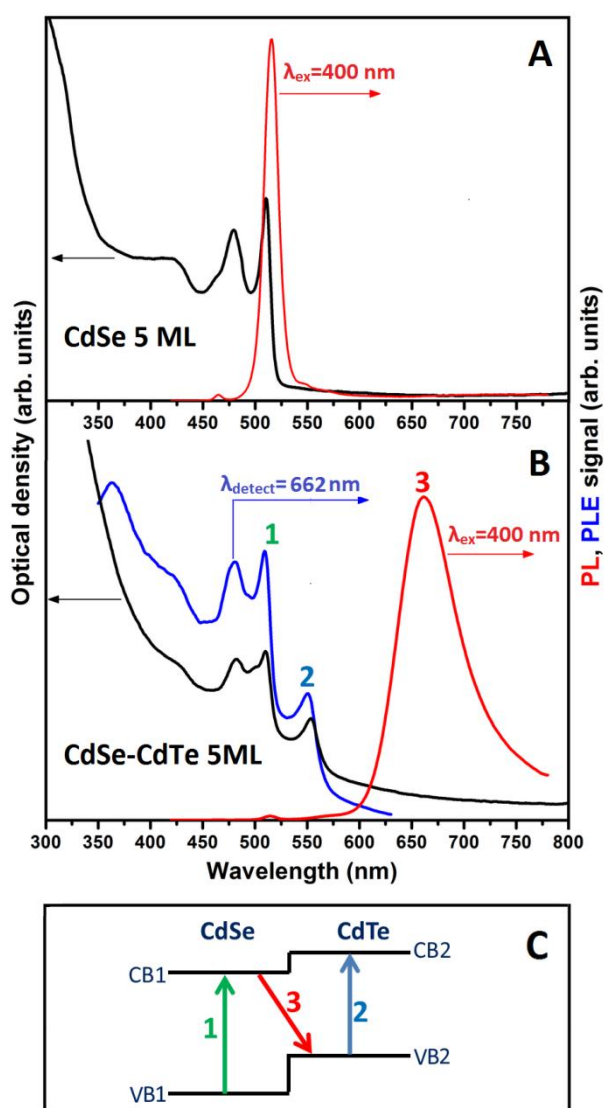


Figure 1. Optical absorption (black lines), PL (red lines) and PLE (blue lines) of bare CdSe 5 ML NPLs (a), CdSe-CdTe core-wings 5 ML hetero-NPLs (b) and schematic diagram demonstrating energy levels and optical transitions in CdSe-CdTe heterostructure (c).

Such relatively high quantum yield indicates that the lateral CdTe overgrowth does not introduce a significant amount of defects or strain in the nanoheteroplatelets. The PL quantum yield may be improved further, e.g. by the growth of gradient structures.⁴¹

It is interesting to compare the optical properties of the CdSe(core)-CdTe(wings) hetero-NPLs with the inverted CdTe(core)-CdSe(wings) structure. However, we failed to prepare 5 ML-thick CdTe NPLs by following the protocol described in ref. 31. Nevertheless, we were able to synthesize 4 ML normal CdSe (core)-CdTe(wings) and inverted CdTe (core)-CdSe (wings) hetero-NPLs (Fig. 2 c,d). They exhibit similar properties to the ones observed for 5 ML CdSe-CdTe NPLs, i.e. the presence of narrow excitonic absorption bands of both CdSe and CdTe NPLs of the same thickness and a PL emission band considerably red-shifted from those of bare

CdSe and CdTe NPLs. As one can expect, the normal and inverted type-II hetero-NPLs with the same thickness exhibit almost identical optical properties. In the PL spectra we observe the bands at $\lambda = 580$ nm for normal 4 ML CdSe-CdTe and $\lambda = 575$ nm for inverted CdTe-CdSe structures (red curve in Figure 2 c,d) (we determined the transition wavelength by a linear fit around the zero-crossing point of the first derivative of the PL or absorption spectrum).

The observed small difference (of 5 nm) of the transition wavelength of the normal and inverted structure may be due to the different lateral sizes of the wing and the core in these hetero-NPLs. In contrast to 5 ML NPLs the PL spectra of 4 ML CdSe and CdTe NPLs possess a large deep trap emission component with a broad band above 600 nm, which is also visible in the PL spectra of either normal CdSe-CdTe or inverted CdTe-CdSe 4 ML hetero-NPLs. Moreover, the position of the deep trap emission in the luminescence spectra of normal CdSe-CdTe and inverted CdTe-CdSe 4 ML hetero-NPLs (Figure 2 c,d) is similar to the deep trap emission for bare CdTe and CdSe NPLs (Figure 2 a,b) respectively. Thus, one can assume that the deep trap emission of hetero-NPLs is caused by defects which are located on the outer edges of nanoplatelets, while trap states on the edges of the inner core are efficiently eliminated by the lateral wing overgrowth similarly to the CdSe-CdS core-wings case.³⁸

The PLE spectra of both hetero-NPLs follow well corresponding absorption spectra, thus pointing to the fact that PL emission derives from NPLs with a CdSe-CdTe heterojunction.

To further substantiate the generation of a type-II junction in the CdSe-CdTe hetero-NPLs we use the spectral position of peak 3 in Figure 1b, which is at 662 nm (1.872 eV). This strongly red-shifted band with respect to those of 5 ML CdTe and CdSe NPLs is due to a transition between electrons localized in the CdSe region and holes in the CdTe region of the heterojunction. Therefore the type-II transition energy is connected to the bandgaps of the attached (inner) CdSe and (outer) CdTe NPLs and their relative band offsets. Using the transition energies (2.430 eV) of our synthesized bare 5 ML CdSe NPLs from a fit, as described above, the transition energy of bare 5 ML CdTe NPLs (2.228 eV) from ref. 33 and the abovementioned hetero-transition energy, we are able to calculate the conduction and valence band offsets in Fig. 1c. A conduction band offset of $\Delta E_C = 0.356$ eV and a valence band offset of $\Delta E_V = 0.558$ eV are obtained (Fig. 3). To ensure that these results are general we performed the same procedure for 4 ML CdSe-CdTe hetero-NPLs using the transition energies of 4 ML CdSe-CdTe, CdSe and CdTe NPLs deduced from fits (as above) to their absorption spectra (Figure 2c).

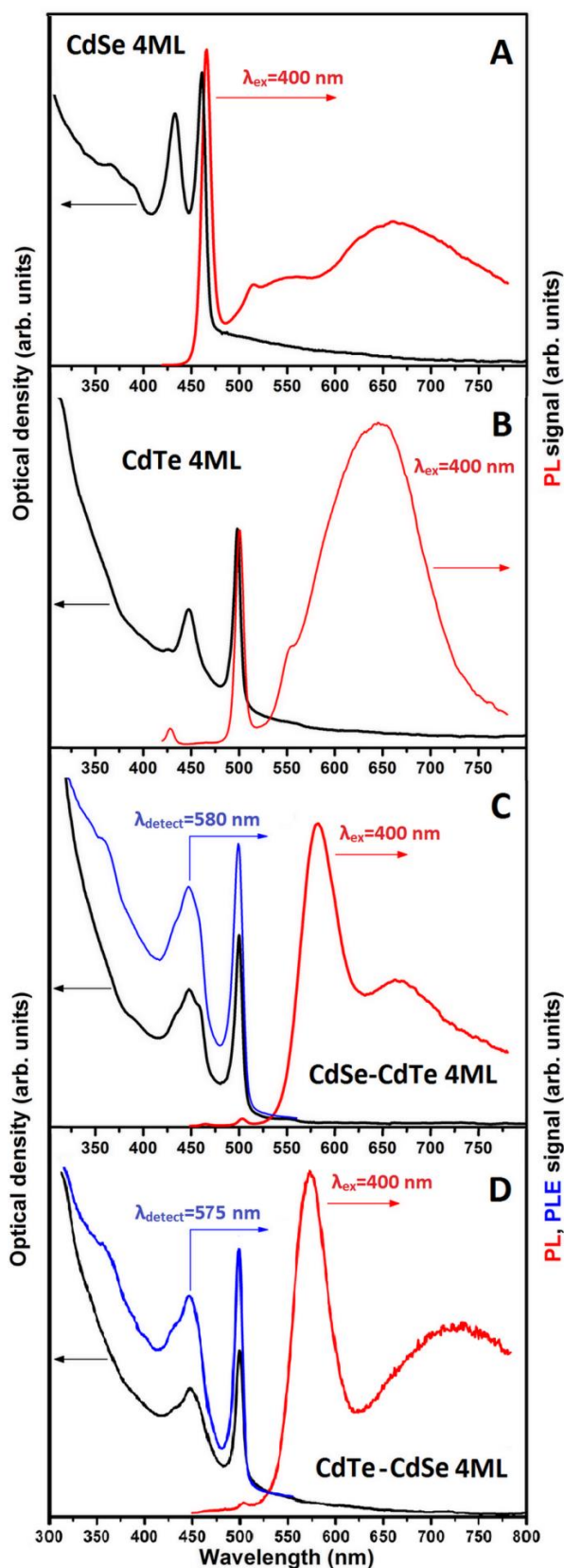


Figure 2. Optical absorption (black lines), PL (red lines) and PLE (blue lines) of bare 4 ML CdSe NPLs (a), bare 4 ML CdTe NPLs (b), “straight” 4ML CdSe(core)-CdTe(wings) hetero-NPLs (c) and “inverted” 4 ML CdTe(core)-CdSe(wings) hetero-NPLs.

The obtained conduction band offset ($\Delta E_C = 0.360$ eV) and valence band offset $\Delta E_V = 0.564$ eV is in very good agreement with the results obtained for the 5 ML case within a 1% error. The very small differences may arise due to very low Fermi level pinning by defects at the interface. Summing up our argumentation the band offsets provide a definite prove of the formation of a type-II junction in our CdSe-CdTe heteronano-platelets.

Moreover the band offsets can be compared with the results of theoretical band offset calculations by Wei et al.⁴⁵ on ZB CdSe and CdTe. They obtained a valence band offset of $\Delta E_V = 0.57$ eV that agrees well with our results. Their conduction band offset of $\Delta E_C = 0.42$ eV deviates from our $\Delta E_C = 0.36$ eV only about 16%. This minor difference may arise from the fact that their calculations are based on bulk values and therefore do not include a confinement induced energetic shift of the conduction band. Calculations by Wang et al.⁴⁶ for CdSe-CdTe heteronano-wires showed, that the confinement results in a reduction of the conduction band offset to $\Delta E_C = 0.28$ with respect to the 0.42 eV bulk value, while the valence band offset is practically unaffected (0.54 eV).

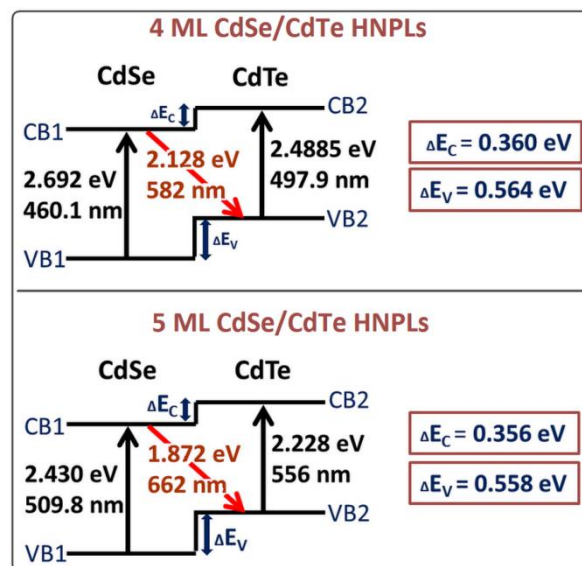


Figure 3. Optical transitions in CdSe-CdTe hetero-NPLs with the transition energies of bare CdSe and CdTe platelets indicated by black arrows and the type-II transitions at the heterojunction indicated by red arrows. The optical transition energies of the 4 and 5 ML CdSe and CdTe platelets and the heterotransition are deduced from fits to the absorption spectra in Figure 1 and the spectra of 4 ML CdSe, CdTe and CdSe-CdTe platelets. The transition energy of 5 ML CdTe platelets was used from ref. 33 since we were not able to synthesize 5ML CdTe platelets.

Electron microscopy

Figure 4 demonstrates HAADF STEM-images of 5 ML CdSe core NPLs before (a) and after (b) their lateral overgrowth with CdTe wings.

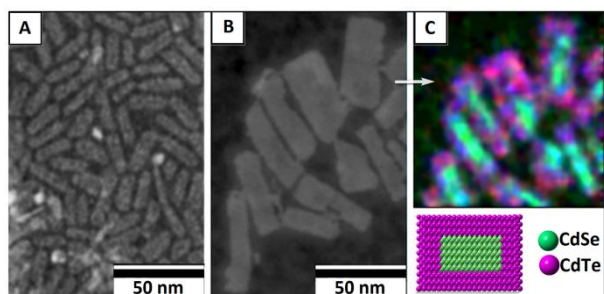


Figure 4. STEM images of 5 ML CdSe core NPLs before (a) and after (b) CdTe overgrowth. c) Color coded EDX map of CdSe-CdTe hetero-NPLs corresponds to the image (b). The 50 nm scale bars are identical in panels A-C.

It can be seen that after the wing deposition procedure the lateral size of the core NPLs increases in all directions that is consistent with the previous observation on the preparation of CdSe-CdS core-wings NPLs.³⁸ Furthermore, the assumption that upon the addition of Cd- and Te-precursors the growth of CdTe phase occurs only at the edges of CdSe NPLs and the aforementioned size increase does not relate to a recrystallization of the initial core NPLs is unambiguously confirmed by a colour coded EDX map (Figure 4c) of the final CdSe-CdTe NPLs.

Figure 5 demonstrates HAADF-STEM-images of 4 ML CdTe core NPLs before (a) and after (b) their lateral overgrowth with CdSe wings along with EDX elemental mapping for inverted CdTe-CdSe 4 ML hetero-NPLs (c). It can be seen that CdTe-CdSe 4 ML hetero-NPLs have a more irregular shape than 5 ML-thick NPLs. This may be attributed to the fact that thinner NPLs are can be assumed to be more susceptible to the twisting and tearing in solution.⁴⁷

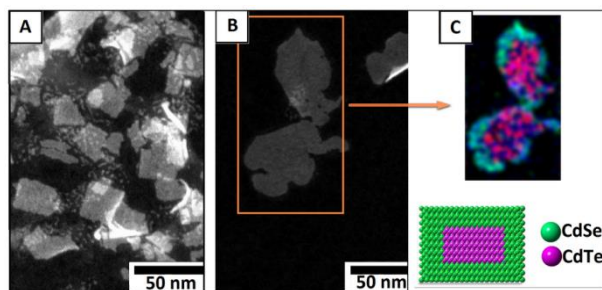


Figure 5. STEM images of 4 ML CdTe core NPLs before (a) and after (b) CdSe overgrowth. c) Color coded EDX map of CdTe-CdSe hetero-NPLs corresponds to the image (b). The 50 nm scale bars are identical in panels A-C.

XRD and EDX

In order to observe changes in elemental and phase composition of NPLs quantitatively, we conducted XRD and EDX analysis of CdSe-CdTe hetero-NPLs (see, Fig. S1 in the Supplementary Information). As a result of the lateral CdTe overgrowth we observe a Te-containing phase. The appearance of signal from sulphur is due to the treatment of the synthesized CdSe-CdTe hetero-NPLs with thiols in order to increase their stability in air.

The corresponding X-ray diffraction patterns of the initial CdSe and CdSe-CdTe hetero-NPLs are shown in Figure 6. It can be seen, that for the core CdSe nanoplatelets only characteristic reflexes of the zinc blende CdSe phase appear. These peaks are considerably broadened because of the finite structure size and slightly shifted to smaller 2θ values due to an increase of the lattice constant as compared to bulk CdSe. The cadmium telluride overgrowth leads to the appearance of new peaks which can be assigned to zinc blende CdTe phase. These new reflexes are accompanied by a small shift of the CdSe reflexes to higher angles due to shrinkage of CdSe lattice. It should be outlined that the (220) and (311) reflexes from the same lattice planes for zinc blende CdSe and CdTe are observed as separate peaks. This indicates that during the lateral CdTe overgrowth no considerable alloying occurs, while otherwise according to Vegard's law each two peaks would appear as one at an intermediate position. However the superposition of the two close reflex families of CdSe and CdTe smears over the spectrum a bit.

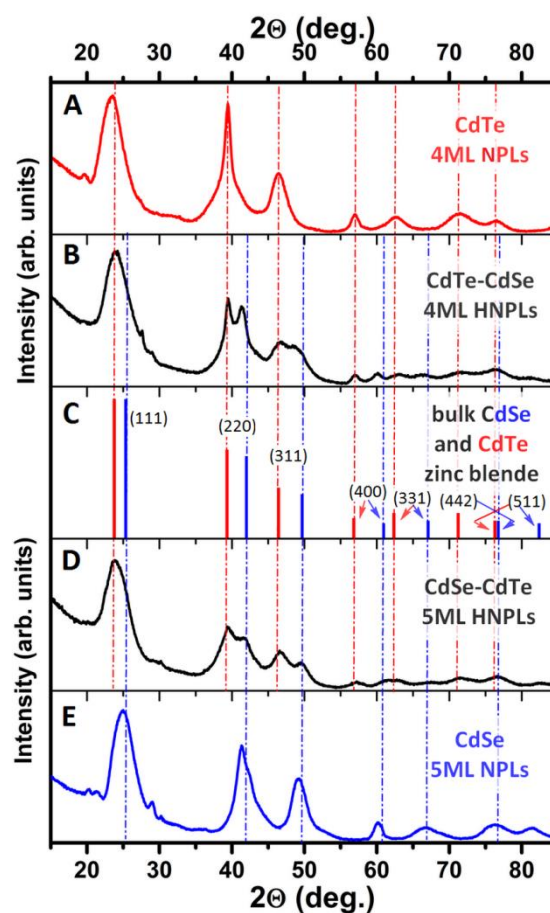


Figure 6. Powder XRD-patterns of 4 ML core CdTe NPLs (a), inverted 4 ML CdTe-CdSe hetero-NPLs (b), 5 ML CdSe-CdTe hetero-NPLs (d) and 5 ML core CdSe NPLs (e). Panel (c) shows reference data for the position and relative intensity of XRD reflexes for bulk zinc-blende CdSe (blue) and CdTe (red).

PL lifetime measurements

In order to investigate the PL dynamics of our core and hetero-NPLs the time-resolved fluorescence measurements with detection at the corresponding core- and hetero-transition peaks were conducted. The resulting decay curves for bare CdSe NPLs, CdSe-CdS type-I and CdSe-CdTe type-II “core-wings” hetero-NPLs are presented in Figure 7. The CdSe-CdS “core-wings” NPLs were prepared by a procedure reported in ref. 38. Corresponding optical absorption, PL and PLE spectra are provided in Figure S2 in the Supplementary Information. Additionally we performed time-resolved measurements for the inverted 4 ML CdTe-CdSe type-II hetero-NPLs.

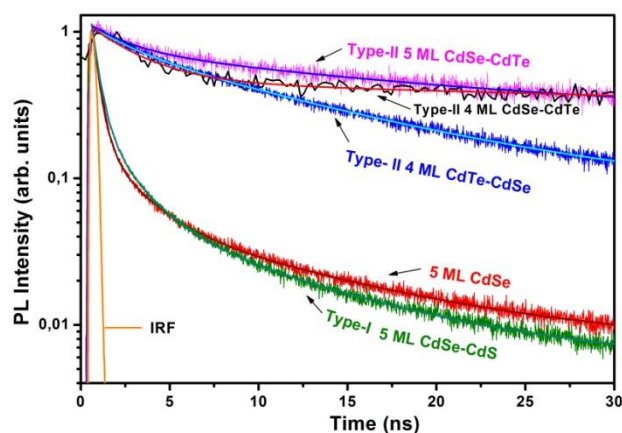


Figure 7. PL decay curves for core 5 ML CdSe NPLs (red) and 5 ML “core-wings” CdSe-CdS type-I (green) and 5 ML CdSe-CdTe type-II (magenta) hetero-NPLs, 4 ML CdSe-CdTe (black) and 4 ML inverted CdTe-CdSe hetero-NPLs (blue). PL decays were measured at the fundamental band gap emission for core and type-I platelets and at the type-II transition energy for all type-II platelets.

The type-II samples exhibit double exponential decays as shown in the fits in Fig. 7. These biexponential PL decays result from an intercombination of the two lowest lying, emitting exciton states (dark and bright states) of CdSe⁴⁸ and CdTe platelets at the hetero junction. For the CdSe and CdSe-CdS we also tried biexponential fitting again taking the convolution with the instrument response into account. However we obtained not fully satisfactory fits. Therefore, we were suggested to do triexponential fits during the review process. These fits are displayed in Figure 7. To our understanding triexponential fits may be reasoned by the following arguments: The first two fast PL decay components can be in this case attributed to the fast dark-bright state dynamics of the nanoplatelets, whereas the third longer component may be the result of shallow defects with much higher lifetime. Fitting the PL decays of our type-II hetero-NPLs instead of the used biexponential with triexponential functions resulted in an artificial 3rd decay component, which did not improve the fit’s chi square. To obtain a comparable measure for the decay constants of all nanoparticles, we use the average lifetime, calculated as⁴⁸

$$\langle \tau \rangle = \sum_i \frac{A_i \tau_i^2}{\sum_j A_j \tau_j} \quad (1)$$

with decay channel amplitudes A_i and decay constants τ_i . The measured $\langle \tau \rangle$ were 2.3 ns for 5 ML CdSe core NPLs, 2.2 ns for 5 ML type-I CdSe-CdS hetero-NPLs and a much longer decay time of 98 ns for the type-II 5 ML CdSe-CdTe hetero-NPLs. The 4 ML type-II CdSe-CdTe hetero-NPLs have a similar decay time of 38 ns, whereas the inverted 4 ML CdTe-CdSe hetero-NPLs are characterized by a shorter average decay time of 18 ns (the larger noise in black decay curve is due to the lower intensity signal which required larger spectral frame for the signal collection). Table 1 lists the fit results for our five samples.

It can be seen that the PL decay of core only and the type-I CdSe-CdS hetero-NPLs with type-I band alignment is characterized by comparable PL decay times $\langle \tau \rangle$. From this we can conclude, that the electronic system of the CdSe NPLs is altered only insignificantly by the introduction of a lateral CdS wings. This is due to the fact that the core platelet lateral size is much larger than the 2D exciton Bohr radius in CdSe (~3 nm).³⁴ Therefore the addition of a lateral CdS wings leads to only minor alteration of the electronic system.

Table 1. Calculated average lifetime $\langle \tau \rangle$ according to Equation (1) for bi(tri-)exponential fittings of PL decay curves in Fig. 7.

Sample	$\langle \tau \rangle$ (ns)
5ML CdSe	2.3
5 ML CdSe-CdS	2.2
5ML CdSe-CdTe	98
4ML CdSe-CdTe	38
4ML CdTe-CdSe	18

Both CdSe and CdSe-CdS NPLs are characterized by a rather fast PL decay ($\langle \tau \rangle \sim 2$ ns) due to the 2D Giant Oscillator Strength (GOST) for direct excitons.⁴⁹ In contrast CdSe-CdTe type-II hetero-NPLs show a prolongation of the average lifetime by a factor of about 50. Similar extended PL decay times for type II CdSe-CdTe hetero-NPLs as compared to core CdSe NPLs were observed also in refs. 41-43, while the exact $\langle \tau \rangle$ values may vary within the different batches due to complex nature of the structure and defect states in hetero-NPLs. However, no data for inverted CdTe-CdSe hetero-NPLs were presented before. The thinner 4 ML inverted CdTe-CdSe hetero-NPLs show also prolonged exciton lifetime characteristic for a type-II transition. The increase in exciton lifetime is related to spatially indirect exciton formation and recombination at the hetero-interface. Since a spatially indirect exciton has a lower electron-hole wavefunction overlap, the transition oscillator strength is lower and hence the exciton lifetime increases. The same argument is valid for both the normal CdSe-CdTe and inverted CdTe-CdSe hetero-NPLs. Comparing the PL lifetimes of straight and inverted 4 ML

hetero-NPLs we see that the different symmetry of the electronic system and the wavefunctions (electrons are mainly confined to the CdSe at the hetero junction, whereas holes are staying in the CdTe (Fig. 3) leads to a longer lifetime of the 4ML CdSe-CdTe hetero-NPLs as compared to inverted 4ML CdTe-CdSe hetero-NPLs. The latter have an apparently slightly stronger confined electronic system, as can be seen by the relative blue shift of the type-II PL emission in Figure 2d with respect to Fig. 2c, which may directly visible in the PL decay time data due to the increased e-h wavefunction overlap resulting in a decreased PL lifetime.

Further we suggest that for the hetero-NPLs the band offsets (~ 0.3 - 0.5 meV) rather than the dark-bright splitting of the order of a few meV⁵⁰ determine the exciton recombination dynamics at the type-II heterointerface. These band offsets may be also responsible for the observed spectral red shift of the luminescence with respect to bare CdTe, CdSe NPLs emission. However, the average exciton lifetimes of our CdSe-CdTe and CdTe-CdSe hetero-NPLs are still shorter than the ones reported e.g. for hetero CdSe-CdTe type-II nanorods (~ 1 μ s),⁵¹ which is a result of the reduction of lifetimes by the 2D Giant Oscillator strength³⁴. Since, our platelets have a relatively large lateral size and hence, increased coherence volume,^{34,47} the GOST effect also leads to shorter lifetimes as compared to Ref. 41. Due to relatively high PL quantum yield in our samples (23%) for the 5 ML CdSe-CdTe hetero-NPLs we can definitely exclude the idea that the observed fast exciton lifetimes in our type-II hetero-NPLs result from dominating non-radiative processes since $\tau_{\text{dec}} = \tau_{\text{rad}} \cdot \text{QY}$, so that the measured decay time τ_{dec} cannot be considerably smaller than the radiative lifetime τ_{rad} .

Conclusions

In summary we have investigated the structural and electronic properties of CdSe-CdTe and inverted CdTe-CdSe heteronanoplatelets. We were able to demonstrate that the growth of CdTe or CdSe sidewings on CdSe or CdTe core nanoplatelets, confirmed by STEM-EDX, leads to type-II heteroplatelets with emission energies defined by the bandgaps of the CdSe and CdTe platelets and the characteristic conduction and valence band offsets. Further, we showed that the observed conduction and valence band offsets of 0.36 eV and 0.56 eV are in line with theoretical results for the CdTe-CdSe band alignment and that the presented type-II heteronanoplatelets exhibit efficient spatially indirect exciton recombination. While the exciton lifetime is strongly prolonged in the investigated type-II 2D systems with respect to 2D type-I systems, the occurring 2D Giant Oscillator Strength (GOST) effect still leads to a fast and efficient exciton recombination. This makes CdSe-CdTe heteronanoplatelets interesting candidates for low threshold lasing applications.

Acknowledgements

M.A. acknowledges the CHEMREAGENTS program. A.A. and A.P. acknowledge partial support from X13M-017 grant from

Belarusian foundation for basic science. YR and DM acknowledge support from Project FIS2013-41184-P of the Spanish Ministry of Economy and Competitiveness MINECO. A.A. and U.W. acknowledge the DFG Funding in Frame of the Wo477 project.

Notes and references

^a Institute for Physico-Chemical Problems, Belarusian State University, Leningradskaya str., 14, Minsk 220030, Belarus

^b Centro de Fisica de Materiales (CSIC-UPV-EHU) and Donostia International Physics Center (DIPC), E-20018 Donostia-San Sebastian, Spain

^c Ikerbasque, Basque Foundation for Science, 48011 Bilbao, Spain

^d CIC nanoGUNE, Tolosa Hiribidea, 76, E-20018 Donostia – San Sebastian, Spain

^e Institute of Optics and Atomic Physics, Technical University of Berlin, Strasse des 17. Juni 135, 10623 Berlin, Germany

*E-mail: m_artemyev@yahoo.com

† Electronic Supplementary Information (ESI) available: [details of any supplementary information available should be included here]. See DOI: 10.1039/b000000x/

1. C. de Mello Donegá, *Chem. Soc. Rev.*, 2011, **40**, 1512.
2. A. M. Smith and S. Nie, *Acc. Chem. Res.*, 2010, **43**, 190.
3. P. Reiss, M. Protière and L. Li, *Small*, 2009, **5**, 154.
4. M. A. Hines and P. Guyot-Sionnest, *J. Phys. Chem.*, 1996, **100**, 468.
5. B. O. Dabbousi, J. Rodriguez-Viejo, F. V Mikulec, J. R. Heine, H. Mattoussi, R. Ober, K. F. Jensen and M. G. Bawendi, *J. Phys. Chem. B*, 1997, **101**, 9463.
6. Y. Chen, J. Vela, H. Htoon, J. L. Casson, D. J. Werder, D. A. Bussian, V. I. Klimov and J. A. Hollingsworth, *J. Am. Chem. Soc.*, 2008, **130**, 5026.
7. T.-H. Kim, S. Jun, K.-S. Cho, B. L. Choi and E. Jang, *MRS Bull.*, 2013, **38**, 712.
8. E. Petryayeva, W. R. Algar and I. L. Medintz, *Appl. Spectrosc.*, 2013, **67**, 215.
9. S. Kim, B. Fisher, H.-J. Eisler and M. G. Bawendi, *J. Am. Chem. Soc.*, 2003, **125**, 11466.
10. S. Kumar, M. Jones, S. S. Lo and G. D. Scholes, *Small*, 2007, **3**, 1633.
11. D. Oron, M. Kazes and U. Banin, *Phys. Rev. B*, 2007, **75**, 035330.
12. J. A. Hollingsworth, *Chem. Mater.*, 2013, **25**, 1318.
13. R. Osovsky, D. Cheskis, V. Kloper, A. Sashchiuk, M. Kroner and E. Lifshitz, *Phys. Rev. Lett.*, 2009, **102**, 197401.

14. V. I. Klimov, S. A. Ivanov, J. Nanda, M. Achermann, I. Bezel, J. A. McGuire and A. Piryatinski, *Nature*, 2007, **447**, 441.
15. H. McDaniel, P. E. Heil, C.-L. Tsai, K. K. Kim and M. Shim, *ACS Nano*, 2011, **5**, 7677.
16. T. O'Connor, M. S. Panov, A. Mereshchenko, A. N. Tarnovsky, R. Lorek, D. Perera, G. Diederich, S. Lambright, P. Moroz and M. Zamkov, *ACS Nano*, 2012, **6**, 8156.
17. S. Kim, Y. T. Lim, E. G. Soltesz, A. M. De Grand, J. Lee, A. Nakayama, J. A. Parker, T. Mihaljevic, R. G. Laurence, D. M. Dor, L. H. Cohn, M. G. Bawendi and J. V. Frangioni, *Nat. Biotechnol.*, 2004, **22**, 93.
18. C. J. Dooley, S. D. Dimitrov and T. Fiebig, *J. Phys. Chem. C*, 2008, **112**, 12074.
19. H. McDaniel, J.-M. Zuo and M. Shim, *J. Am. Chem. Soc.*, 2010, **132**, 3286.
20. H. McDaniel, M. Pelton, N. Oh and M. Shim, *J. Phys. Chem. Lett.*, 2012, **3**, 1094.
21. S. Liu, W. H. Zhang and C. Li, *J. Cryst. Growth*, 2011, **336**, 94.
22. N. Oh, S. Nam, Y. Zhai, K. Deshpande, P. Trefonas and M. Shim, *Nat. Commun.*, 2014, **5**, 1.
23. J. E. Halpert, V. J. Porter, J. P. Zimmer and M. G. Bawendi, *J. Am. Chem. Soc.*, 2006, **128**, 12590.
24. D. J. Milliron, S. M. Hughes, Y. Cui, L. Manna, J. Li, L.-W. Wang and A. P. Alivisatos, *Nature*, 2004, **430**, 190.
25. S. W. Tong, N. Mishra, C. L. Su, V. Nalla, W. Wu, W. Ji, J. Zhang, Y. Chan and K. Loh, *Adv. Funct. Mater.*, 2014, **24**, 1904.
26. S. Schmitt-Rink, D. S. Chemla and D. A. B. Miller, *Adv. Phys.*, 1989, **38**, 89.
27. S. S. Lo, T. Mirkovic, C.-H. Chuang, C. Burda and G. D. Scholes, *Adv. Mater.*, 2011, **23**, 180.
28. C. Bouet, M. D. Tessier, S. Ithurria, B. Mahler, B. Nadal and B. Dubertret, *Chem. Mater.*, 2013, **25**, 1262.
29. S. A. Cherevkov, A. V. Fedorov, M. V. Artemyev, A. V. Prudnikau and A. V. Baranov, *Phys. Rev. B*, 2013, **88**, 041303.
30. Z. Li, H. Qin, D. Guzun, M. Benamara, G. Salamo and X. Peng, *Nano Res.*, 2012, **5**, 337.
31. S. Pedetti, B. Nadal, E. Lhuillier, B. Mahler, C. Bouet, B. Abécassis, X. Xu and B. Dubertret, *Chem. Mater.*, 2013, **25**, 2455.
32. E. Lhuillier, S. Pedetti, S. Ithurria, B. Nadal, H. Heuclin and B. Dubertret, *Acc. Chem. Res.*, 2015, **48**, 22.
33. S. Ithurria, M. D. Tessier, B. Mahler, R. P. S. M. Lobo, B. Dubertret and A. L. Efros, *Nat. Mater.*, 2011, **10**, 936.
34. A. W. Achtstein, A. Schliwa, A. Prudnikau, M. Hardzei, M. V. Artemyev, C. Thomsen and U. Woggon, *Nano Lett.*, 2012, **12**, 3151.
35. C. She, I. Fedin, D. S. Dolzhenkov, A. Demortière, R. D. Schaller, M. Pelton and D. V. Talapin, *Nano Lett.*, 2014, **14**, 2772.
36. B. Mahler, B. Nadal, C. Bouet, G. Patriarche and B. Dubertret, *J. Am. Chem. Soc.*, 2012, **134**, 18591.
37. S. Ithurria and D. V. Talapin, *J. Am. Chem. Soc.*, 2012, **134**, 18585.
38. A. Prudnikau, A. Chuvilin and M. V. Artemyev, *J. Am. Chem. Soc.*, 2013, **135**, 14476.
39. B. Guzelurk, Y. Kelestemur, M. Olutas, S. Delikanli and H. V. Demir, *ACS Nano*, 2014, **8**, 6599.
40. L. T. Kunneman, J. M. Schins, S. Pedetti, H. Heuclin, F. C. Grozema, A. J. Houtepen, B. Dubertret and L. D. a Siebbeles, *Nano Lett.*, 2014.
41. S. Pedetti, S. Ithurria, H. Heuclin, G. Patriarche and B. Dubertret, *J. Am. Chem. Soc.*, 2014, **136**, 16430.
42. Y. Kelestemur, M. Olutas, S. Delikanli, B. Guzelurk, M. Z. Akgul and H. V. Demir, *J. Phys. Chem. C*, 2015, **119**, 2177.
43. K. Wu, Q. Li, Y. Jia, J. R. McBride, Z. Xie and T. Lian, *ACS Nano*, 2015, **9**, 961.
44. S. Ithurria, G. Bousquet and B. Dubertret, *J. Am. Chem. Soc.*, 2011, **133**, 3070.
45. S.-H. Wei, S. B. Zhang and A. Zunger, *J. Appl. Phys.*, 2000, **87**, 1304.
46. S. Wang and L.-W. Wang, *J. Phys. Chem. Lett.*, 2010, **2**, 1.
47. E. M. Hutter, E. Bladt, B. Goris, F. Pietra, J. C. van der Bok, M. P. Boneschanscher, C. de Mello Donegá, S. Bals and D. Vanmaekelbergh, *Nano Lett.*, 2014, **14**, 6257.
48. M. Jones, S. S. Lo and G. D. Scholes, *J. Phys. Chem. C*, 2009, **113**, 18632.
49. J. Feldmann, G. Peter, E. Göbel, P. Dawson, K. Moore, C. Foxon and R. Elliott, *Phys. Rev. Lett.*, 1987, **59**, 2337.
50. L. Biadala, F. Liu, M. D. Tessier, D. R. Yakovlev, B. Dubertret and M. Bayer, *Nano Lett.*, 2014, **14**, 1134.
51. M. Jones, S. Kumar, S. S. Lo and G. D. Scholes, *J. Phys. Chem. C*, 2008, **112**, 5423.